Dalton Transactions

Dynamic Article Links ►

Cite this: 2013, 42, 10315-10325.

PAPER

www.rsc.org/xxxxxx

Homo- and Heterometallic Planes, Chains and Cubanes‡

Seán T. Meally,[a] Stephanie M. Taylor,[b] Euan K. Brechin,[b] Stergios Piligkos[c]* and Leigh F. Jones[a]*

Received (in XXX, XXX) Xth XXXXXXXXX 20XX, Accepted Xth XXXXXXXXX 20XX

DOI: 10.1039/b000000x

The synthesis, structural and magnetic characterisation of a family of homo- and heterometallic complexes constructed with the Schiff base ligands 2-iminomethyl-6-methoxy-phenol (L_1H) and 2-imino-6-methoxy-phenol (L_2H), are discussed. Members include the heterometallic tetranuclear complexes of general formula $[Na_2M_2(X)_2(L_1)_4(Y)_2]$ (where M = Fe^{III}, X = $^{-}$OMe, Y = NO_3^- (**1**) and M = Ni^{II}, X = N_3^- and Y = MeCN (**2**)), each possessing a butterfly-like topology. We also report the formation of the heterometallic molecular cage $[Na_3Ni_2(L_1)_6](ClO_4)$ (**3**) whose metallic skeleton describes a [rare] trigonal bipyramid, the homometallic 1-D coordination polymer $[Mn(L_1)_2(Cl)]_n$ (**4**), and the tetranuclear cubane clusters $[Mn^{III}_3Mn^{IV}(O)_3(OEt)(OAc)_3(L_1)_3]$ (**5**) and $[Ni_4(\mu_3\text{-}OMe)_4(L_2)_4(MeOH)_4]$ (**6**). *Dc* and *ac* magnetic susceptibility studies on complexes **5** and **6** reveal $S = 9/2$ and $S = 4$ spin ground states.

Introduction

The field of coordination chemistry regularly provides examples of fascinating homo- and heterometallic molecules with potential applications in disparate fields. For instance in bioinorganic chemistry certain heterometallic manganese complexes have been proposed as biomimetic models for energy and electron transfer processes - one such stimulus being the bimetallic $[Mn_4CaO_4]$ cubane-like catalytic unit within photosystem II (PSII).[1] Mn has also played a pivotal role in the field of molecular magnetism: the anisotropic nature of the Mn^{III} ion means that it is regularly selected as the metal of choice in the synthesis of Single-Molecule Magnets (SMMs)[2] and Single-Chain Magnets (SCMs),[3] whilst the isotropic Mn^{II} ion is often employed in the construction of molecular magnetic refrigerants.[4] This field has also seen a rennaisance in the synthesis of heterometellic 3*d*/4*f* cluster compounds, driven, in the main, by the tuneable anisotropy of the lanthanide ions,[5,6] offering the chemist the opportunity to vary the physical properties of a molecule without altering its structure. Moreover the deliberate inclusion of diamagnetic metal ions, including 2*p* (Na^I, K^I, Ca^{II}, Mg^{II}), 3*d* (Zn^{II}) and 4*f* (La^{III})) ions within large molecular architectures can also afford the chemist vital insights into the magneto-structural relationship, by allowing the elucidation of the magnitude and sign of specific M-L-M magnetic exchange pathways when directly compared to their paramagnetic analogues.[7] Herein we describe how we are able to produce both homo- (3*d*) and heterometallic (2*p*-3*d*) polynuclear complexes depending on the specific reaction conditions employed. We describe firstly the synthesis and magnetic characterisation of two tetranuclear mixed-metal complexes of general formula $[Na_2M_2(X)_2(L_1)_4(Y)_2]$ (where M = Fe^{III}, X = $^{-}$OMe, Y = NO_3^- (**1**) and M = Ni^{II}, X = N_3^- and Y =MeCN (**2**)). Each possess a butterfly-like metallic skeleton stabilised by the deprotonated Schiff base ligand 2-iminomethyl-6-methoxy-phenol (L_1H; Scheme 1). This ligand is then used in the construction of the heterometallic trigonal bipyramidal complex $[Na_3Ni_2(L_1)_6](ClO_4)$ (**3**) and the homometallic chain $[Mn(L_1)_2(Cl)]_n$ (**4**). We then describe the synthesis of two structurally similar homometallic $[M_4]$ cubane complexes $[Mn^{III}_3Mn^{IV}(O)_3(OEt)(OAc)_3(L_1)_3]$ (**5**) and $[Ni_4(\mu_3\text{-}OMe)_4(L_2)_4(MeOH)_4]$ (**6**) (where L_2H is 2-imino-6-methoxy-phenol; Scheme 1), both of which are produced *via* slight pertubations to the synthetic procedures employed to make **1** and **2**.

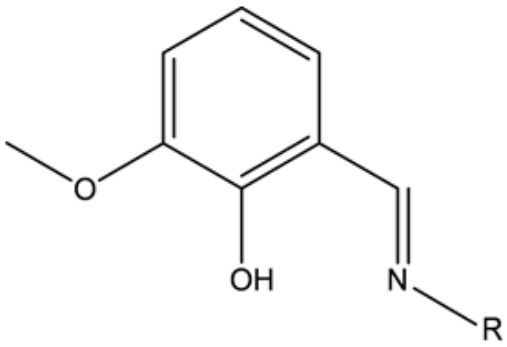

Scheme 1. The structures of L_1H (R = CH_3) and L_2H (R = H).

Results and Discussion

Our previous research with the L_1H ligand produced a family of heptanuclear $[M_7]$ (M = Ni^{II}, Zn^{II}, $Co^{II/III}$) pseudo metallocalix[6]arene complexes whose structures give rise to the

formation of H-bonded molecular host cavities which are shown to accommodate numerous guest species in the solid state.[8,9] Building on this work and diversifying towards other 1st-row transition metals we have found that the reaction of an Fe^{III} or Ni^{II} salt ($FeCl_3{\cdot}6H_2O$ or $[Fe_3O(O_2CPh)_6(MeOH)_3](NO_3)$ in **1** and $Ni(NO_3)_2{\cdot}6H_2O$ in **2**) with L_1H and a suitable base (NaOH or NaOMe) produces the butterfly complexes $[Na_2Fe_2(OMe)_2(L_1)_4(NO_3)_2]{\cdot}2MeOH$ (**1**) and $[Na_2Ni_2(\mu_3\text{-}N_3)_2(L_1)_4(MeCN)_2]$ (**2**). The structures of **1** and **2** (Figure 1) are isostructural, each crystallising in the monoclinic $P2_1/n$ space group, and will therefore be described collectively. Selected interatomic distances and angles for all complexes are listed in Tables S1-3. Tables 1 and 2 contain all relevant crystallographic data for **1**-**6**. The planar diamond or buttefly-like core of **1** and **2** comprises two 1st-row transition metal centres situated at the central or body positions connected to two outer or wing-tip Na^+ ions, to form a near planar rhombic core (Fig. 1). Such topologies in homometallic tetranuclear cluster complexes ($[M_4]$ (M = 1st-row transition ions) are well documented in the literature, predominantly in Mn and Fe chemistry,[10,11] although other 1st-row transition metals have been incorporated into this motif.[12] The formation of heterometallic Na^+-3*d* butterflies is less common, examples include $[Na_2Fe_2(O\textit{t}Bu)_6(thf)_2]$,[13] $[\{(tmeda)Na(R)(OBu)(o\text{-}C_6H_4OMe)Mn\}_2]$ (where tmeda = N,N,N',N'-tetramethylethylenediamine),[14] $\{CrCax[6](O)_3(OH)_3Na(NCMe)_2(\mu\text{-}OH)\}_2{\cdot}4MeCN$ (where Cax[6] = *p-tert*-butylcalix[6]arene)[15] and $[Na_2Co_2(\mu_3\text{-}O\textit{t}Bu)_2(\mu_2\text{-}O\textit{t}Bu)_4(thf)_2]$.[16] Examples of 3*d*-4*f* butteflies of general formula $[Co^{II}_2Ln^{III}_2]$ have more recently been reported with the $[Co_2Gd_2]$ member of this family exhibiting SMM behaviour.[17]

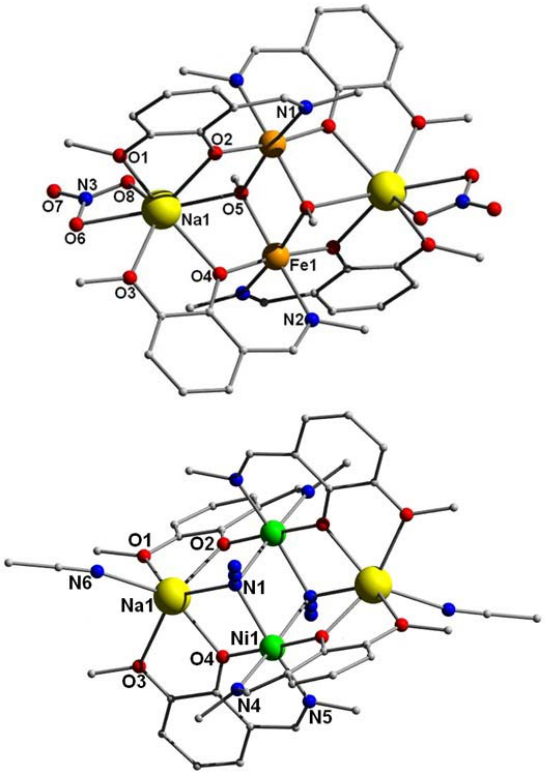

Figure 1 The molecular structures of the bimetallic butterfly-like complexes **1** and **2**. Colour code: Orange (Fe); Green (Ni); Yellow (Na); Blue (N); Red (O); Grey (C). Hydrogen atoms omitted for clarity. Fe1-O5-Fe1' = 101.41°, Fe···Fe = 3.133 Å; Ni1-N1-Ni' = 99.75°, Ni···Ni = 3.352 Å.

In both **1** and **2** an inversion centre is located at the midway point between the two paramagnetic centres occupying the central body positions. In each case the four metal centres are linked by μ_3-bridging ions, $^-$OMe in **1** and 'end-on' (EO) μ_3-1,1,1-N_3^- ions in **2**. The L_1^- ligands are singly deprotonated (*via* loss of the phenolic proton) and link the wing-tip ions to the central body metal ions, bridging in a $\eta^1{:}\eta^2{:}\eta^1{:}\mu$-fashion (Fig. 1). The four L_1^-ligands lie alternately above and below the near planar core formed by the four metal centres. The central μ_3-bridging ions lie out of the $[Na_2M_2(\mu_3\text{-}L)_2]$ plane as illustrated in Fig. S1. The coordination spheres of the wing-tip metals are completed by the chelating NO_3^- ions (**1**) and neutral MeCN solvent molecules (**2**). Each buttefly complex possesses Na^+ ions at the wing-tip positions of their $[Na_2M_2(\mu_3\text{-}L)_2]$ cores; those in **2** exhibit a six coordinate octahedral geometry, while those in **1** are seven coordinate with the additional bonds arising from the chelating NO_3^- ions. The distorted octahedral Fe^{III} and Ni^{II} ions in **1** and **2** possess $\{N_2O_4\}$ and $\{N_4O_2\}$ coordination spheres respectively, with bond length ranges of 1.944 – 2.156 Å in **1** and 2.004 – 2.176 Å in **2**. The formation of complex **2** represents only the second example of an EO μ_3-1,1,1-N_3^- bridged 2*p*-3*d* butterfly complex[18] and was produced by introducing NaN_3 into the $Ni(NO_3)_2{\cdot}6H_2O$ / L_1H / NaOH reaction mixture to give rhomb shaped crystals of **2** in ~10% yield (Figures 2 and S5). Indeed the azide ligand (N_3^-), when bridging paramagnetic transition metal centres in the EO μ_3-1,1,1-N_3^- bonding motif, is often known to promote ferromagnetic coupling, although this appears to be dependent on the M-N-M angle.[19] In the crystals of **2** there are no intra- or inter-molecular H-bonding interactions but there are numerous inter-molecular short contacts. For example, the bridging azides interact with $-CH_3$ protons (H10B and H20C) belonging to the L_1^- ligands of an adjacent $\{Na_2Ni_2\}$ cluster (N3···H10B = 2.611 Å, N3···H20C = 2.655 Å). Long contacts are also observed between the six coordinate body Na^+ ions (Na1 and symmetry equivalent. s.e.) and nearby $-CH_3$ protons (H1A and s.e) on adjacent cluster units at a distance of 3.192 Å. These inter-molecular interactions occur in all three directions to give the brickwork packing motif shown in Figure S2.

On closer scrutiny of the crystal structure of **1** it becomes apparent that there are numerous inter-molecular H-bonding interactions. The non-bonded O-atom (O7, Figure 1) of the chelating NO_3^- anion H-bonds with protons of neighbouring L_1^- ligands belonging to three separate $[Na_2Fe_2]$ units; O7···H17(C17) = 2.545 Å, O7···H8(C8) = 2.464 Å, O7···H3(C3) = 2.559 Å. Further contacts occur between the bonded NO_3^- O-atoms with juxtaposed L_1^- ligands, O6···H18A(C18) = 2.542 Å and O8···H17A(C17) = 2.545 Å. These multiple inter-molecular interactions link the individual $[Na_2Fe_2]$ units into superimposable chains which traverse the *bc* plane of the unit cell (*via* the acceptor atoms O6, O7 and O8). These individual hydrogen bonded chains are then linked *via* the aformentioned O7···H-C interactions in both the two remaining directions (Fig. S2).

Table 1 Crystallographic data for complexes **1-4**

	1	**2**	**3**	**4**
Formula[a]	$C_{40}H_{52}N_6O_{18}Na_2Fe_2$	$C_{40}H_{46}N_{12}O_8Na_2Ni_2$	$C_{54}H_{60}N_6O_{16}ClNa_3Ni_2$	$C_{18}H_{20}N_2O_4ClMn$
M_W	1062.56	986.29	1270.92	418.75
Crystal System	Monoclinic	Monoclinic	Trigonal	Monoclinic
Space group	$P2_1/n$	$P2_1/n$	P-3	C2/c
a/Å	11.6905(5)	11.663(2)	13.808(2)	14.731(3)
b/Å	11.1560(5)	11.884(2)	13.808(2)	12.851(3)
c/Å	19.0629(9)	15.975(3)	17.308(4)	9.6901(19)
α/°	90	90	90	90
β/°	93.391(4)	98.72(3)	90	106.66(3)
γ/°	90	90	120	90
V/Å^3	2481.82(19)	2188.5(8)	2857.8(8)	1751.3(6)
Z	2	2	2	4
T/K	150(2)	150(2)	150(2)	150(2)
λ[b]/Å	0.7107	0.7107	0.7107	0.7107
D_c/g cm^{-3}	1.422	1.497	1.477	1.583
μ(Mo-Ka)/ mm^{-1}	0.677	0.946	0.802	0.930
Meas./indep.(R_{int}) refl.	4336 / 2737 (0.0956)	3991 / 3584 (0.0171)	2834 / 2239 (0.0267)	1610 / 1374 (0.0657)
wR2 (all data)[c]	0.2723	0.0674	0.2471	0.1716
$R1$[d,e]	0.0966	0.0255	0.1108	0.0655
Goodness of fit on F^2	1.082	1.108	1.288	1.067

[a] Includes guest molecules.[b] Mo-Kα radiation, graphite monochromator. [c] $wR2= [\Sigma w(|F_o^2| - |F_c^2|)^2 / \Sigma w|F_o^2|^2]^{1/2}$. [d]For observed data. [e] $R1= \Sigma||F_o| - |F_c|| / \Sigma|F_o|$.

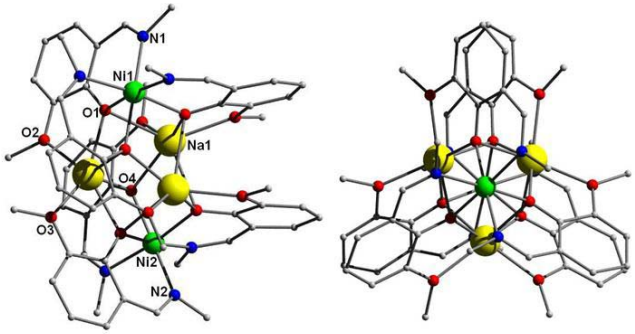

Figure 2 (Left) The molecular structure of **3**. (Right) The molecular structure of **3** viewed along the Ni···Ni vector of the $[Na_3Ni_2]$ trigonal bipyramidal core, highlighting the pseudo three-fold symmetry. H-atoms are omitted for clarity.

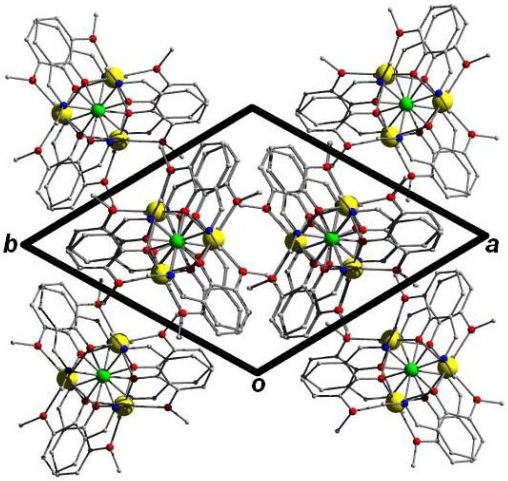

Figure 3 Crystal packing observed in **3** as viewed along the *c* axis of the unit cell. H-atoms are omitted for clarity.

Replacement of NO_3^- with ClO_4^- in the Ni^{II} / L_1H / NaOH reaction mixture used in the synthesis of **2** gives rise to an altogether different species: the heterometallic pentanuclear complex $[Na_3Ni_2(L_1)_6](ClO_4)$ (**3**), which crystallises in the trigonal *P*-3 space group. The structure of **3** (Figure 2) comprises a trigonal bipyramidal core of metal ions in which the three 6-coordinate Na^+ ions (Na1 and s.e) of distorted octahedral geometry occupy the equatorial positions, and the two Ni^{II} (Ni1 and Ni2) ions (also in distorted octahedral geometries) are located in the two axial positions. The six L_1^- anions each span one of the six axial Ni···Na vertices of the trigonal bipyramidal core, employing the rather unusual $\eta^1{:}\eta^3{:}\eta^1,\mu_3$-bonding mode. More specifically, the phenoxide O-atoms (O1 and O4) link the axial Ni^{II} centres to the equatorial Na^+ ions as well as forming bridges between the Na^+ ions around the equatorial plane of the molecule (Fig. 2). An inversion centre is located at the centre of the triangle formed by the three equatorial Na^+ ions. The Na-O bond distances lie in the 2.26-2.69 Å range, while a sole ClO_4^- counter anion balances the charge of the $[Na_3Ni_2(L_1)_6]^+$ unit. The ClO_4^- anion lies on a pseudo C_3 axis (D_{3h} symmetry of core when L_1^- ligands are ignored) directly above the Ni^{II} ions and are positioned alternately in between the individual $[Na_3Ni_2]$ moieties propagating -$[Na_3Ni_2]$-$[ClO_4]$-$[Na_3Ni_2]$- 1-D chains along the *c* axis of the unit cell (Figures 3 and 4). These chains are stabilised by numerous hydrogen bonding interactions between the perchlorate O-atoms (O5, O6 and s.e) and the $-CH_3$ protons of four nearby L_1^- ligands (two from each $[Na_3Ni_2]$ unit sandwiching the ClO_4^- anions (Fig. 4)). Complex **3** represents the first example of a trigonal bypyramidal $[Na_3Ni_2]$ species although a similar La^{III} complex, $[La_2Na_3(\mu_4\text{-}OR)_3(\mu\text{-}OR)_6(THF)_5]$ is known.[20]

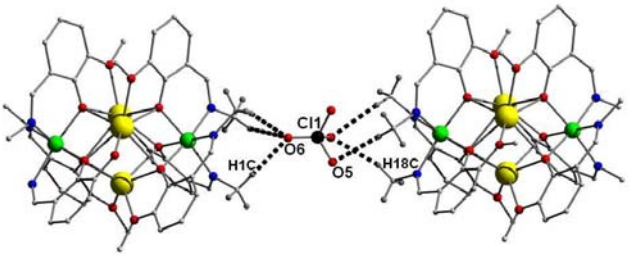

Figure 4 Section of the $[Na_3Ni_2]^{\cdots}[ClO_4]^{\cdots}[Na_3Ni_2]$ 1-D chains observed in the crystal structure of **3**. Dashed lines represent H-bonds at distances H1C···O6 = 2.349 Å, H18C···O5 = 2.520 Å.

Interestingly the presence of the Mn^{III} ion, formed *in situ* via the aerial oxidation of $MnCl_2{\cdot}4H_2O$ in the presence of [L_1H and] NEt_4OH, gives rise to the formation of the homometallic 1-D coordination polymer $[Mn(L_1)_2(Cl)]_n$ (**4**) (Figure 5). Here two singly deprotonated L_1^- ligands chelate the Mn^{III} ion at its equatorial positions while its Jahn-Teller elongated bonds are provided by two symmetry equivalent Cl^- ions (Mn1-Cl1 = 2.676 Å). These chloride ions act as linker ligands to adjacent Mn^{III} ions to form the covalent zig-zag chain structure shown in Figure 5. The chains propagate along the *c* axis of the cell and pack in the familiar brickwork formation (Fig. S3).

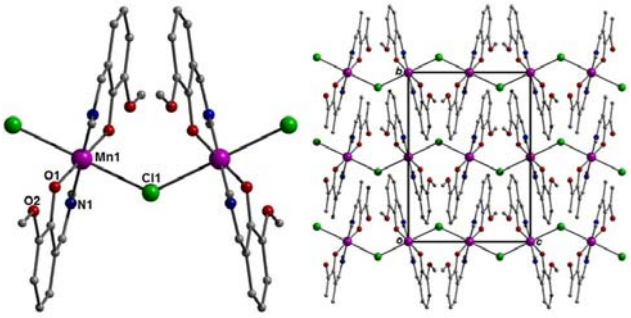

Figure 5 (left) Two $\{Mn(L_1)_2(Cl)\}$ units within the 1-D chain in **4**. (Right) Packing in **4** as viewed along the *a* axis of the unit cell. Hydrogen atoms omitted for clarity.

It is clear that the common thread running through the formation of the heterometallic $[Na_2M_2]$ complexes **1** and **2** and the trigonal bipyramidal complex $[Na_2Ni_3]$ (**3**) is the presence of the Na^+ ion, which originates from the use of NaOH. Indeed the use of an organic base, NEt_4OH, affords the homometallic $[Mn(L_1)_2(Cl)_2]$ (**4**) chain. In order to investigate this further, the reactivity of the Schiff base ligand L_1H in the presence of a variety of different bases, and in the complete absence of base, was studied. After numerous attempts we found that the reaction of $Mn(OAc)_2.4H_2O$ with L_1H in EtOH for a period of 24 hours, produced black X-ray quality crystals of the tetrametallic complex $[Mn^{III}_3Mn^{IV}(O)_3(OEt)(OAc)_3(L_1)_3]$ (**5**) in the orthorhombic space group $P2_12_12_1$ (Figure 6). Its core can be described as a highly distorted $\{Mn_4O_4\}$ cubane which, when viewed along the Mn1-O13 vertex, exhibits psuedo three-fold symmetry. The Mn centres occupy alternate corners of the distorted cube. Mn-O bond lengths, bond valence sum (BVS) calculations (Table S4) and charge balance considerations, reveal that Mn1 is in the +IV oxidation state and that Mn2-4 are in the +III oxidation state. The latter display the expected Jahn-Teller elongations [2.182(3) – 2.250(4) Å] which all lie perpendicular to each other and all share O13 (Fig. 6).

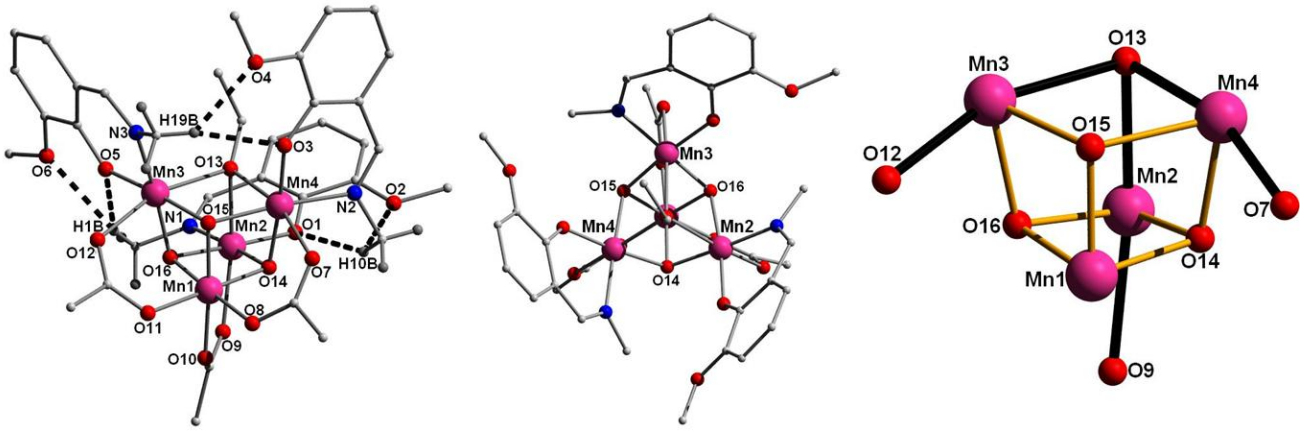

Figure 6: (left) Crystal structure of **5**. Dashed lines represent the intra-molecular H-bonds at distances (Å): H19B···O4 = 2.375, H19B…O3 = 2.516, H10B···O2 = 2.547, H10B···O1 = 2.414, H1B···O5 = 2.497, H1B ···O6 = 2.660; (centre) View of the pseudo C_s axis in complex **5**; (right) The cubane core in **5** highlighting (dark lines) the mutually orthogonal Jahn-Teller elongation axes.

Crystal System	Orthorhombic	Tetragonal
Space group	$P2_12_12_1$	$I4_1/a$
a/Å	11.6508(4)	22.187(3)
b/Å	16.9627(6)	22.187(3)
c/Å	20.6910(7)	9.5524(19)
α/°	90	90
β/°	90	90
γ/°	90	90
V/Å^3	4089.1(2)	4702.1(13)
Z	4	4
T/K	150(2)	150(2)
λ^b/Å	0.7107	0.7107
D_c/g cm^{-3}	1.596	1.537
μ(Mo-Ka)/ mm^{-1}	1.280	1.648
Meas./indep.(R_{int}) refl.	6272/4611 (0.0599)	2060/1134 (0.0934)
wR2 (all data)	0.1168	0.1184
$R1^{d,e}$	0.0544	0.0572
Goodness of fit on F^2	1.001	0.811

The Mn centres are linked into the cubane topology *via* three μ_3-O^{2-} ions (O14, O15 and O16) and one μ_3-bridging $^-$OEt ligand (O13) to give Mn-O-Mn angles ranging from 88.84 to 111.06°. The three $^-$OAc ligands each bridge two Mn centres across one face of the cubane in the common η^1:η^1:μ-bonding motif. The three L_1^- ligands are singly deprotonated and simply chelate Mn2, Mn3 and Mn4 at three of the four corners of the cube. By chelating to the Mn^{III} ions Mn2, Mn3 and Mn4, the three L_1^- ligands form a shallow cavity [of approximate dimensions 3.72 × 9.90 × 4.33 Å; (base × rim × height)] of which the Mn2 / Mn3 / Mn4 plane forms its triangular base (Fig. 6). The triply bridging ethoxide ion sits inside this cavity (Figure 7). Closer inspection of the crystal structure in **5** shows evidence of multiple intra-molecular H-bonding interactions involving the three L_1^- ligands. More specifically, each ligand forms four H-bonds with its nearest neighbour *via* their N-CH_3 methyl protons and juxtaposed -OCH_3 and O_{phen}-atoms (dashed lines in Figure 6). The [Mn_4O_4] cubane units arrange into superimposable 1-D rows down the *a* axis, which, in the *bc* plane, are assembled in the common brickwall pattern (Fig. S4). Complex **5** joins a small family of analogous mixed valence [$Mn^{III}_3Mn^{IV}$] cubanes which include the previously reported SMMs [$Mn^{III}_3Mn^{IV}O_3(X)(OAc)_3(dbm)_3$] (where X = Cl^-, Br^-; dbm = dibenzoylmethane)[1c] and [$Mn^{III}_3Mn^{IV}O_3(O_2CR)_4(dbm)_3$] (R = CH_3, Ph).[21]

The formation of complex **5** illustrates that the addition of a [relatively] strong base in such reactions is not imperative, but a base of some sort – even the acetate present in the starting material – appears to be required. Reactions in the absence of base produced no isolable products for any other paramagnetic 1st-row transition metal. Previous work employing strong bases in L_1H/Ni^{II} chemistry led to the formation of a family of heptanuclear pseudo metallocalix[6]arene complexes.[8a,b] Use of NaOMe in place of NaOH, however, produces the tetranuclear Ni^{II} cubane [$Ni_4(\mu_3$-$OMe)_4(L_2)_4(MeOH)_4$] (**6**; Figure 8). Alkoxide-bridged Ni^{II} cubanes are a well-known class of compound.[22] Crystals of **6** form in the tetragonal $I4_1/a$ space group and its cationic [$Ni_4(\mu_3$-$OMe)_4]^{4+}$ core is comparable to that in [Mn_4] (**5**), comprising a distorted cubane core with the Ni^{II} centres (Ni1 and s.e) occupying alternate corners of the cube. They are connected *via* four μ_3-bridging $^-$OMe ions (O2 and s.e) producing Ni1-O2-Ni1 angles ranging from 96.50 to 98.32°, while the four singly deprotonated L_2^- ligands chelate the four metal centres. The distorted octahedral geometries of the metal ions are completed by terminal MeOH solvent molecules (Fig. 8). The alcoholic protons of the latter (H1 and s.e) partake in intra-molecular H-bonding with O_{phen} atoms of a nearby L_2^- ligand (O3) at a distance of O1(H1)···O3 = 1.896 Å. The individual [Ni_4] units in **6** form superimposable 1-D rows along the *c* axis of the cell, which are packed into a grid-like arrangement when viewed in the *ab* plane (Fig. 9). This packing motif is propagated by numerous crystallographically equivalent inter-molecular interactions. More specifically each [Ni_4] moiety has eight C-H···O interactions *via* the aromatic protons (H3) and methoxy oxygen atoms (O4) of the four symmetry equivalent L_2^- ligands (C3(H3)…O4 = 2.447 Å). Interestingly [$Ni_4(\mu_3$-$OMe)_4(L_1)_4(MeOH)_4$], despite much effort, cannot be made. A potential reason for this apparent anomaly soon becomes clear on looking more closely at the structure of **6**. The only difference between ligands L_1H and L_2H is the absence of an –CH_3 imine

group on the latter. This C=NH imine group (labelled as N1-H1 on L_2H in **6**) lies in close proximity to the adjacent bridging μ_3-OEt ligand (labelled C10-O2) at a distance of only N1(H1)···H10A(C10) = 2.329 Å.[23] Thus, the replacement of L_2H with L_1H in **6** is likely implausible due to the steric constraints the C=N-CH_3 methyl group would impose on the system.

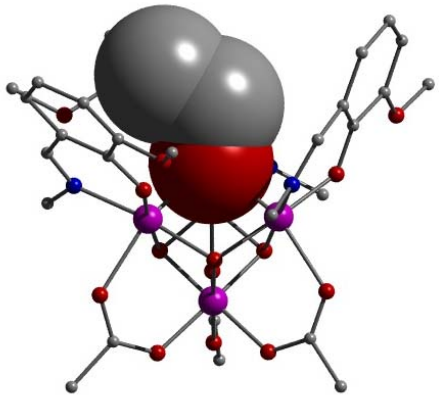

Figure 7 Space-fill representation of the μ_3-bridging $^{-}$OEt ligand which sits within a molecular cavity forged by the three L_1^- ligands in **5**.

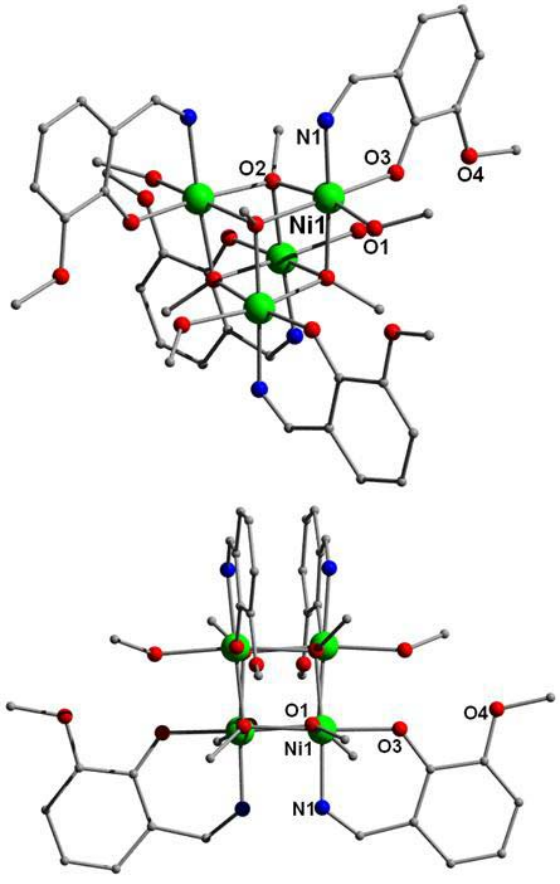

Figure 8 Crystal structure of **6** as viewed off-set (top) and aligned (bottom) with one of the cube faces. H-atoms have been omitted for clarity.

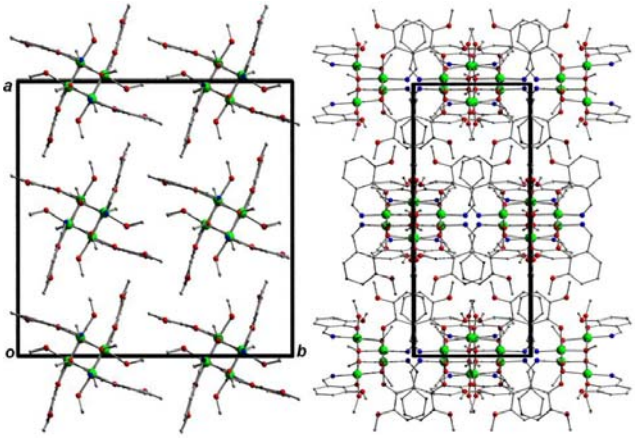

Figure 9 Crystal packing diagrams of **6** viewed along the *c* (left) and *b* (right) axes.

Magnetic Susceptibility Studies

The *dc* molar magnetic susceptibilities, χ_M, of polycrystalline samples of **1**, **2**, **4**, **5**, and **6**, were measured in an applied magnetic field, *B*, of 0.1 T over the 5 to 300 K temperature (*T*) range. The experimental results for complex **1** are shown in Figure 10 in the form of the $\chi_M T$ product, where $\chi = M/B$ and *M* is the magnetisation of the sample. At 300 K, the $\chi_M T$ product of **1** has a value of 6.36 cm^3 mol^{-1} K, significantly lower than the expected spin-only value of 8.75 cm^3 mol^{-1} K (for $g = 2.0$). On cooling, the $\chi_M T$ product drops, reaching 0.11 cm^3 mol^{-1} K at 5 K. This behaviour is indicative of antiferromagnetic exchange between the Fe^{III} centres in **1**. We have used the isotropic spin-Hamiltonian (1) to model the magnetic properties of complex **1**:

$$\hat{H}_{iso} = -2\sum_{i,j>i} J_{ij}\,\hat{S}_i \cdot \hat{S}_j + \mu_B B \sum_i g_i \hat{S}_i \qquad (1)$$

where *i* and *j* are integers that index the constitutive single-ions in **1**, *J* is the isotropic exchange interaction parameter, $\hat{S}$ is a spin operator, μ_B is the Bohr magneton and *g* is the *g*-factor. Spin-Hamiltonian (1) is given here in a general form because it will be used in further sections to model the magnetic properties of complexes **2**, **4**, **5** and **6**. For the numerical diagonalisation of the matrix representation of spin-Hamiltonian (1), for all studied complexes, we used home written software (ITO-MAGFIT[24]) and spin-Hamiltonian (1) was fitted to the experimental data by use of the Levenberg–Marquardt algorithm.[25] For **1**, this resulted in the best-fit parameter: $J_{Fe\text{-}Fe}$ = -6.4 cm^{-1}, keeping the *g*-value of Fe^{III} fixed to g_{Fe} = 2. These values are comparable with previously reported alkoxide-bridged Fe^{III} dimers containing similar Fe-O-Fe angles and Fe···Fe distances.[26] The obtained best-fit curve is shown as a solid line in Figure 10.

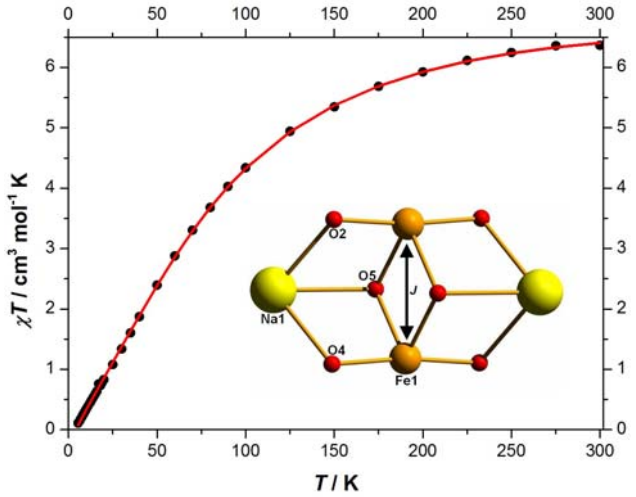

Figure 10 Plot of $\chi_M T$ vs. T of **1**. Inset: the magnetic exchange scheme employed in the fitting of **1**. The solid red line represents best fit curve to the experimental data.

The *dc* molar magnetic susceptibility data for **2** are shown in Figure 11. The room temperature $\chi_M T$ product of 2.10 cm^3 mol^{-1} K is slightly higher than that expected from the spin-only contributions from two non interacting Ni^{II} centres (2.0 cm^3 mol^{-1} K for $g = 2$). Upon cooling, the $\chi_M T$ product of **2** rises to reach a maximum of 3.74 cm^3 mol^{-1} K at 17 K. This behaviour is indicative of ferromagnetic exchange between the constitutive Ni^{II} ions. Below 17 K, the $\chi_M T$ product of **2** decreases to reach 3.61 cm^3 mol^{-1} K at 5 K (Figure 11). To better determine the low temperature behaviour of **2**, variable-temperature-variable-field (VTVH) magnetisation data were collected on polycrystalline samples of **2** (Figure 11, inset), in the temperature and field ranges 2 to 7 K and 0.5 to 7.0 T, respectively. The $\chi_M T$ product of **2** was numerically fitted to spin-Hamiltonian (1), in the same way as for **1**, to yield the best fit parameter: $J_{Ni\text{-}Ni}$ = 8.0 cm^{-1}, keeping the *g*-value of Ni^{II} fixed to g_{Ni} = 2.2, this *g*-value being the one that provides the best agreement with experiment when g_{Ni} is varied in the interval g_{Ni} = 2.0 to g_{Ni} = 2.2. The obtained best-fit curve, which also includes corrections for diamagnetism (of the order of -2 x 10^{-3} cm^3 mol^{-1}) that make the calculated $\chi_M T$ product fall slightly below the experimental value at room temperature, is shown in Figure 11 as a solid line. For the fitting of the VTVH magnetisation data of **2**, we used spin-Hamiltonian (2):

$$\hat{H}_{aniso} = \hat{H}_{iso} + \sum_i D_i(\hat{S}_{z,i}^2 - S_i(S_i+1))/3 \qquad (2)$$

where $\hat{H}_{iso}$ refers to spin-Hamiltonian (1), D is the uniaxial anisotropy parameter of centre i (Ni^{II} for **2**) and S the total spin of centre i (S = 1 for **2**). Spin-Hamiltonian (2) was fitted to the experimental data by use of the simplex algorithm,[25] to give the best-fit parameter D_{Ni} = -4.0 cm^{-1} or, with comparable goodness of fit, as measured by the X^2 statistics, D_{Ni} = +5.7 cm^{-1}, $J_{Ni\text{-}Ni}$ being kept fixed to the best-fit value obtained by fitting of the $\chi_M T$ product of **2**. Thus, the sign, and to a lesser extent the magnitude, of the uniaxial anisotropy parameter, D_{Ni}, is undetermined by fitting of the VTVH thermodynamic magnetisation data of **2**. To determine the sign and magnitude of D_{Ni} with more precision, spectroscopic methods such as Electron

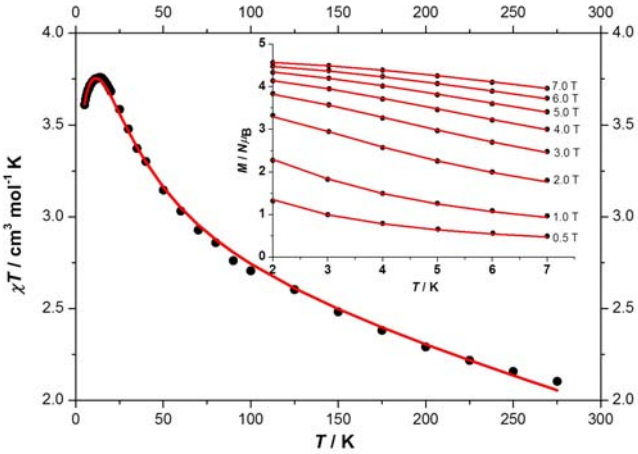

Figure 11 Plot of $\chi_M T$ vs. T of **2**. Inset: Low temperature magnetisation vs. temperature (at various magnetic fields) plot of **2**. Solid red lines represent best fit to the experimental data.

Paramagnetic Resonance should be employed. The best-fit curves to the VTVH magnetisation data of **2** are shown as solid lines in the inset of Figure 11.

The *dc* molar magnetic susceptibility data for **4** are shown in Figure 12 in the form of $\chi_M T$ product per $\{Mn(L_1)_2(Cl)\}$ unit. The room temperature $\chi_M T$ product of 2.64 cm^3 mol^{-1} K is lower than that expected from the spin-only contribution for a single Mn^{III} ion (3.0 cm^3 mol^{-1} K for g = 2). Upon cooling the $\chi_M T$ product of **4** drops reaching 0.09 cm^3 mol^{-1} K at 5 K. This behaviour is indicative of antiferromagnetic exchange between neighbouring Mn^{III} centres in **4**. Interpretation of the magnetic properties of **4** by an exact quantum treatment is impossible since, except for the case of antiferromagnetically coupled spin-half chains,[27] there exists no analytical solution for the general case of this problem for infinite systems. Thus, for the interpretation of the magnetic properties of **4**, we used an approach based on the extrapolation to infinity of the results obtained by exact numerical diagonalisation of the matrix representation of spin-Hamiltonian (1) on model ring systems of increasing size. This strategy was first used in the pioneering work by Bonner and Fischer[28] and more recently for the interpretation of the magnetic properties of fluoride bridged Mn^{III} chains.[29] The model systems that we use are rings consisting of Mn^{III} ions that are antiferromagnetically coupled only to their first neighbours *via* the monoatomic Cl^- bridges. The nuclearity of these model systems ranges from 2 to 9. Our analysis was limited to nuclearity 9 because we block-diagonalise spin-Hamiltonian (1) by exploiting only the symmetries related to the total spin, S, and its projection along the quantization axis, S_z. For model rings containing more than 9 Mn^{III} centres, exact matrix diagonalisation as implemented in ITO-MAGFIT,[24] is not possible. Furthermore, we have fited spin-Hamiltonian (1) against the experimental data only in the temperature range 300 to 20 K to avoid anisotropic terms, of the type expressed in spin-Hamiltonian (2), becoming important. The

best-fit curve obtained for a model system of nuclearity 9, is shown as a solid line in Figure 12. The best-fit curves for model systems of nuclearity less than 9 are very similar to the one shown in Figure 12. In the inset of Figure 12 are shown the best-fit $J_{Mn\text{-}Mn}$ parameters for model systems of varying nuclearity in

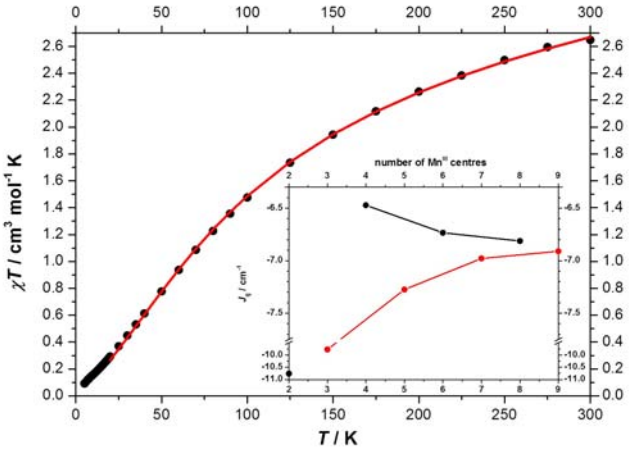

Fig 12 Plot of $\chi_M T$ vs. T of **4**. Inset: Best-fit magnetic exchange interaction, J, for Mn^{III} chains of variable nuclearity (2 to 9).

the range 2 to 9. Notice, that for odd and even nuclearity model systems, the best-fit $J_{Mn\text{-}Mn}$ parameters converge asymptotically to a limit value but from different sides of this limit, expressing the fact that at infinity, there is no difference between odd and even nuclearity and that the limit value at infinity is the same irrespective of the parity. In addition, one should notice that the dinuclear model system does not behave like an even mebered ring. The best-fit $J_{Mn\text{-}Mn}$ parameter for the 8- and 9-member rings are -6.8 and -6.9 cm^{-1}, respectively. Thus, the best-fit $J_{Mn\text{-}Mn}$ parameter for **4** lies within this interval.

The *dc* molar magnetic susceptibility data for **5** are shown in Figure 13. The room temperature $\chi_M T$ product of 9.21 cm^3 mol^{-1} K is lower than that expected from the spin-only contributions for a $[Mn^{IV}Mn^{III}_3]$ moiety (10.88 cm^3 mol^{-1} K for g_{Mn} = 2). Upon cooling, the $\chi_M T$ product of **5** rises to reach a maximum of 11.52 cm^3 mol^{-1} K at 70 K, before decreasing thereafter to a value of 9.70 cm^3 mol^{-1} K at 5 K. This behaviour is suggestive of competing ferromagnetic and antiferromagnetic exchange interactions. The $\chi_M T$ product of **5** was numerically fitted to spin-Hamiltonian (1) to yield the best fit parameters: $J_{Mn(IV)\text{-}Mn(III)}$ = -5.22 cm^{-1} and $J_{Mn(III)\text{-}Mn(III)}$ = 5.26 cm^{-1}, keeping the g-value of Mn^{III} and Mn^{IV} fixed to g_{Mn} = 2.0 (see Fig. S6 for the model scheme employed). The obtained best-fit curve is shown in Figure 13 as a solid line. Under these conditions the ground spin-state of **5** is an S = 9/2 spin-state, as expected for this class of compounds.[1c,20] As in the case of **2**, to better determine the low temperature behaviour of **5,** VTVH magnetisation data were colected on a polycrystalline powder sample of **5** (Figure 13, inset), in the temperature and field ranges 2 to 7 K and 0.5 to 7.0 T, respectively. Spin-Hamiltonian (2) was fitted to the experimental VTVH magnetisation data of **5** as previously described. The best-fit parameters were D_{MnIII} = -1.75 cm^{-1} and $D_{Mn(IV)}$ = 0.81 cm^{-1}, $J_{Mn(IV)\text{-}Mn(III)}$ and $J_{Mn(III)\text{-}Mn(III)}$ being kept fixed to the best-fit values obtained by fitting of the $\chi_M T$ product. The best-fit curves to the VTVH magnetisation data of **5** are shown as solid lines in the inset of Figure 13.

The *dc* molar magnetic susceptibility data for **6** are shown in Figure 14. The room temperature $\chi_M T$ product of 5.80 cm^3 mol^{-1} K is higher than that expected from the spin-only contributions for four non-interacting Ni^{II} centres (4.84 cm^3 mol^{-1} K for g_{Ni} = 2.2), pointing towards ferromagnetic interactions between the constituent Ni^{II} centres. Upon cooling, the $\chi_M T$ product of **6** rises

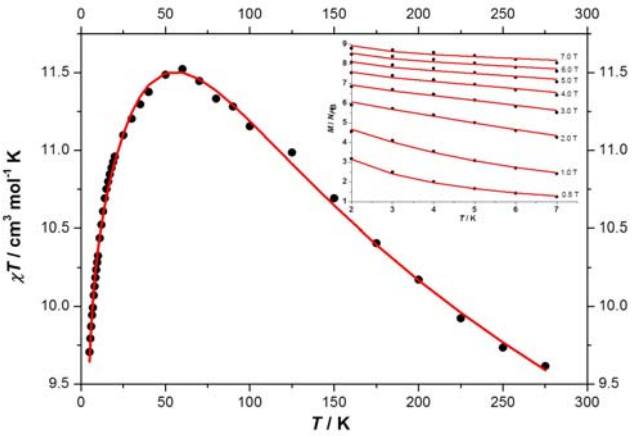

Fig 13 Plot of $\chi_M T$ vs. T of **5**. Inset: Low temperature magnetisation vs. temperature (at various magnetic fields) plot of **5**. Solid red lines represent best fit to the experimental data.

to reach a maximum of 13.06 cm^3 mol^{-1} K at 14 K, before decreasing to a value of 12.34 cm^3 mol^{-1} K at 5 K. This behaviour is indicative of ferromagnetic interactions operating in **6**, the low temperature decrease of the $\chi_M T$ product of **6** probably being due to the uniaxial anisotropy of Ni^{II}, $D_{Ni(II)}$. The $\chi_M T$ product of **6** was numerically fitted to spin-Hamiltonian (1) to yield the best fit parameter: $J_{Ni\text{-}Ni}$ = 5.6 cm^{-1}, keeping the g-value of Ni^{II} fixed to g_{Ni} = 2.2 (see Fig. S6 for the model scheme employed). The obtained best-fit curve is shown in Figure 14 as a solid line. Under these conditions the ground spin-state of **6** is an S = 4 spin-state. To better determine the low temperature behaviour of **6**, VTVH magnetisation data were collected on a polycrystalline sample of **6** (Figure 14, inset), in the temperature and field ranges 2 to 7 K and 0.5 to 7.0 T, respectivelly. Spin-Hamiltonian (2) was fitted to the experimental VTVH magnetisation data of **6**, as previously described. The best-fit parameter was $D_{Ni(II)}$ = 4.6 cm^{-1}, $J_{Ni\text{-}Ni}$ being kept fixed to the best-fit value obtained by fitting of the $\chi_M T$ product of **6**. The best-fit curves to the VTVH magnetisation data of **6** are shown as solid lines in the inset of Figure 14. It should be noted here that the sign, and to a lesser extent the magnitude, of the uniaxial anisotropy parameter, D_{Ni}, is undetermined by fitting of the VTVH thermodynamic magnetisation data of **6**. To determine the sign and magnitude of D_{Ni} with more precision, spectroscopic methods such as electron paramagnetic resonance should be employed.

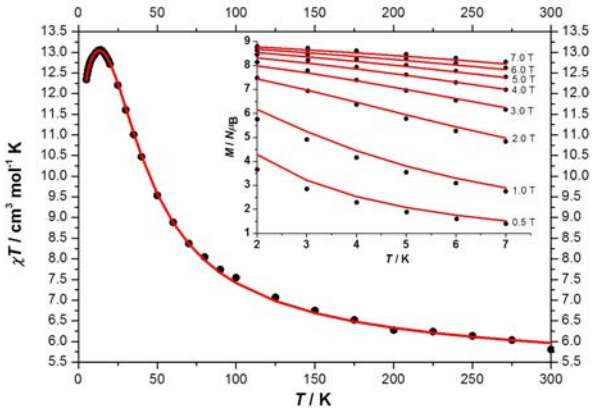

Fig. 14 Plot of $\chi_M T$ vs. T of **6**. Inset: Low temperature magnetisation vs. temperature (at various magnetic fields) plot of **6**. Solid red lines represent best fit to the experimental data.

Concluding Remarks

We have shown how reactions of the Schiff base ligand 2-iminomethyl-6-methoxy-phenol (L_1H) with the 1st-row transition metal ions Fe^{III} and Ni^{II} form the heterometallic complexes $[Na_2Fe_2(OMe)_2(L_1)_4(NO_3)_2]$ (**1**) and $[Na_2Ni_2(\mu_3\text{-}N_3)_2(L_1)_4(MeCN)_2]$ (**2**). In each case the $\{Na_2M_2\}$ cores can be described as possessing near planar butterfly-like topologies with the Na^+ and M^{x+} (Fe^{III} (**1**) and Ni^{II} (**2**)) ions occupying the wing-tip and body positions, respectively. The introduction of the perchlorate anion into the reaction mixture gives rise to the trigonal bipyramidal cage complex $[Na_3Ni_2(L_1)_6](ClO_4)$ (**3**) in which the paramagnetic Ni^{II} ions lie at the apices of the skeleton and are therefore magentically well separated (Ni1···Ni2 = 5.950 Å). We have also shown that the omission of base and the employment of weaker bases (NaOMe *vs.* NaOH), leads to the formation of the homometallic cubane complexes $[Mn^{III}_3Mn^{IV}(O)_3(OEt)(OAc)_3(L_1)_3]$ (**5**) and $[Ni_4(\mu_3\text{-}OMe)_4(L_2)_4(MeOH)_4]$ (**6**). Magnetic studies of **5** and **6** indicate ground spin states of S = 9/2 and S = 4, respectively. In conclusion we have demonstrated that both major and minor modifications to a reaction synthon, can lead to the formation of wholly different complexes of varying topologies and magnetic properties. Such systematic studies are fundamental to our knowledge base as we rapidly progress in the pre-design era we now enjoy in the field of molecular magnetism.

Experimental Section

Physical measurements

Infra-red spectra were recorded on a Perkin Elmer FT-IR *Spectrum One* spectrometer equipped with a Universal ATR Sampling accessory (NUI Galway). Elemental analysis were carried out by Marion Vignoles and Gerard Fahy of the School of Chemistry microanalysis service at NUI Galway. Variable-temperature, solid-state direct current (*dc*) and alternate current (*ac*) magnetic susceptibility data down to 1.8 K were collected on a Quantum Design MPMS-XL SQUID magnetometer equipped with a 7 T dc magnet (University of Edinburgh). Diamagnetic corrections were applied to the observed paramagnetic susceptibilities using Pascal`s constants.

Materials and syntheses

All reactions were performed under aerobic conditions and all reagents and solvents were used as purchased. ***Caution:*** *Although we encountered no problems care should be taken when using the potentially explosive perchlorate, nitrate and azide salts.* The trinuclear complex $[Fe_3O(O_2CPh)_6(MeOH)_3](NO_3)$[30] and the ligands 2-iminomethyl-6-methoxy-phenol (L_1H)[8] and 2-imino-6-methoxy-phenol (L_2H)[31] were synthesised as previously reported.

$[Na_2Fe_2(OMe)_2(L_1)_4(NO_3)_2]\cdot 2MeOH$ (1)

Method A: To a conical flask (100 cm^3) was added the trinuclear complex $[Fe_3O(O_2CPh)_6(MeOH)_3](NO_3)$ (0.50 g, 0.47 mmol) in MeOH (30 cm^3) and the mixture agitated to dissolve the solid. L_1H (0.08 g, 0.47 mmol) was then added resulting in a colour change from dark orange to deep purple. NaOMe (0.025 g, 0.47 mmol) was then added and the solution agitated for 2 h before being filtered. Dark purple X-ray quality crystals of **1** were obtained after Et_2O diffusion of the mother liquor in ~23% yield. *Method B:* $Fe(NO_3)_3\cdot 9H_2O$ (0.25 g, 0.63 mmol), L_1H (0.102 g, 0.63 mmol) and NaOMe (0.066 g, 1.23 mmol) were dissolved in 30 cm^3 MeOH from which a deep purple solution was obtained after a 4 h stir. The resultant solution was then filtered and diffused with Et_2O to form X-ray quality crystals of **1** in ~20% yield. Elemental analysis (%) calculated for $C_{38}H_{46}N_6O_{16}Fe_2Na_2$: C, 45.62; H, 4.63; N, 8.40; Found: C, 45.21; H, 4.38; N, 8.87. FT-IR: 2972(w), 2925(w), 2820(w), 1621(vs), 1600(s), 1559(m), 1454(m), 1405(m), 1371(s), 1344(vs), 1303(s), 1248(s), 1198(m), 1172(m), 1145(w), 1076(m), 1017(m), 999(m), 971(m), 860(m), 826(w), 781(m), 752(m), 737(m).

$[Na_2Ni_2(N_3)_2(L_1)_4(MeCN)_2]$ (2)

$Ni(NO_3)_2\cdot 6H_2O$ (0.25 g, 0.86 mmol) was dissolved in 25 cm^3 MeOH to which was added 2-iminomethyl-6-methoxy-phenol (L_1H) (0.142 g, 0.86 mmol), NaOH (0.011 g, 1.70 mmol) and NaN_3 (0.112 g, 1.70 mmol). The resultant lime green solution was left to stir for 5 h and then allowed to evaporate to dryness. Bright green X-ray diffraction quality crystals of **2** were obtained upon recrystallisation of the resultant green solid from MeCN *via* both slow evaporation and Et_2O diffusion methods (~10 % yield). Elemental analysis (%) calculated for $C_{40}H_{46}N_{12}O_8Na_2Ni_2$: C, 48.71; H, 4.70; N, 17.04; Found: C, 48.43; H, 4.47; N, 17.44. FT-IR (cm^{-1}): 3050 (w), 2977 (w), 2927 (m), 2895 (m), 2835(w), 2287(w), 2253(w), 2046(vs), 1631(s), 1595(s), 1544 (w), 1476(s), 1454(s), 1432(s), 1403(s), 1392 (s), 1338(s), 1285(m), 1232(m), 1214(s), 1167(m), 1142(m), 1094(m), 1077(s), 971(s), 931(w), 870(w), 858(m), 781(w), 734(s).

$[Na_3Ni_2(L_1)_6](ClO_4)$ (3)

$Ni(ClO_4)_2\cdot 6H_2O$ (0.25 g, 0.68 mmol) was dissolved in 30 cm^3 MeOH to which was added to 2-iminomethyl-6-methoxy-phenol (L_1H) (0.11 g, 0.70 mmol) and NaOH (0.04 g, 1.0 mmol) and the resultant lime green solution left to stir for 4 h. The solution was

then evaporated to dryness and dissolved in 10 cm^3 of CH_2Cl_2. Green block crystals of **3** suitable for X-ray diffraction were obtained in ~30% yield upon Et_2O diffusion. Elemental analysis (%) calculated for $C_{54}H_{60}N_6O_{16}ClNa_3Ni_2$: C, 51.03; H, 4.76; N, 6.61; Found: C, 50.45; H, 4.80; N, 7.02. FT-IR (cm^{-1}): 3063 (w), 2894 (w), 2850 (s), 2789 (w), 1631 (s), 1595 (s), 1547 (w), 1453 (s), 1396 (s), 1319(w), 1213(s), 1168(w), 1142(w), 1077(s), 967(s), 872(w), 851(m), 778(w), 728(s).

$[Mn(L_1)_2Cl]_n$ (4)

$MnCl_2{\cdot}4H_2O$ (0.25 g, 1.26 mmol) and L_1H (0.208 g, 1.26 mmol) were dissolved in 25 cm^3 of EtOH. Upon addition of the base NaOH (0.05 g, 1.25 mmol), the solution went from yellow to black. The black solution obtained was stirred for 4 h at room temperature and then filtered. X-ray quality crystals of **4** were formed after five days upon Et_2O diffusion of the mother liquor (yield = 35%). The red-brown crystals were collected and dried in air. Elemental analysis (%) calculated for $C_{18}H_{20}ClMnN_2O_4$: C 51.61, H 4.78, N 6.69. Found: C 51.30, H 4.74, N 6.40. IR needed: 2975 (w), 2920 (w), 2835 (w), 1618 (s), 1595 (s), 1551 (m), 1472 (w), 1445 (s), 1434 (s), 1401 (m), 1382 (w), 1306 (s), 1254 (s), 1220 (s), 1204 (w), 1172 (w), 1115 (w), 1101 (m), 1078 (s), 1007 (m), 973 (m), 960 (m), 889 (w), 866 (s), 777 (w), 751 (w), 738 (s).

$[Mn^{III}_3Mn^{IV}(O)_3(OEt)(OAc)_3(L_1)_3]$ (5)

$Mn(OAc)_2{\cdot}4H_2O$ (0.245 g, 1.00 mmol) and L_1H (0.164 g, 1.00 mmol) were added to 25cm^3 of EtOH and stirred for 24 h. The resultant black solution was then filtered to give black X-ray quality crystals of **5** upon Et_2O diffusion in ~20% yield after 7 days. Elemental analysis calculated (%) for $C_{35}H_{44}N_3O_{16}Mn_4$: C, 42.79; H, 4.51; N, 4.28; Found: C, 42.59; H, 4.33; N, 4.20. FT-IR (cm^{-1}): IR needed: 2921(w), 2828(w), 1630(m), 1595(w), 1551(s), 1474(w), 1463(w), 1440(s), 1408(m), 1385(w), 1336(w), 1298(s), 1238(s), 1225(s), 1196(w), 1175(w), 1097(w), 1081(m), 1056(w), 1017(m), 972(m), 927(w), 861(s), 787(w), 738(s), 682(w).

$[Ni_4(\mu_3\text{-}OMe)_4(L_2)_4(MeOH)_4]$ (6)

$Ni(NO_3)_2{\cdot}6H_2O$ (0.245 g, 1.00 mmol) and L_2H (0.164 g, 1.00 mmol) were added to 25cm^3 of MeOH and stirred for 4 h. The resultant dark green solution was then filtered to give green X-ray quality crystals of **6** in 20 % yield after 7 days *via* Et_2O diffusion into the mother liquor. Elemental analysis calculated (%) for $C_{40}H_{60}N_4O_{16}Ni_4$: C, 42.79; H, 4.51; N, 4.28; Found: C, 42.59; H, 4.33; N, 4.20. FT-IR (cm^{-1}): 3246(w), 3051(w), 2997(w), 2926(w), 2822(w), 1626(s), 1607(m), 1539(m), 1468(m), 1444(w), 1434(w), 1417(w), 1365(w), 1334(w), 1239(m), 1202(m), 1169(w), 1102(w), 1074(w), 1055(m), 1037(m), 961(m), 943(w), 894(w), 856(w), 785(w), 746(m), 726(m).

X-ray crystallography

Diffraction data on **5** was collected at 150 K on a Bruker Smart Apex CCDC diffractometer, equipped with an Oxford Cryosystems LT device, using Mo radiation. The structures of **1-4** and **6** were collected on an Xcalibur S single crystal diffractometer (Oxford Diffraction) using an enhanced Mo source. Each data reduction was carried out on the CrysAlisPro software package. For more detailed refinement information please consult the ESI. Full details can also be found in the CCDC files 936642-936647.

Acknowledgements

LFJ wishes to thank the NUI Galway Millennium Fund and the Irish Research Council (IRCSET Embark Initiative (SM). EKB thanks the EPSRC and Leverhulme Trust. S.P. thanks the Danish Ministry of Science, Innovation and Higher Education for a Sapere Aude Fellowship (10-081659).

Notes and references

[a] *School of Chemistry, National University of Ireland, Galway, University Road, Galway, Ireland. Tel: +353 091-49- 3462, Email:leigh.jones@nuigalway.ie*

[b] *EaStCHEM School of Chemistry, The University of Edinburgh, West Mains Road, EH9 3JJ, UK*

[c] *Department of Chemistry, University of Copenhagen, Universitetsparken 5, DK-2100, Denmark. Email: piligkos@kiku.dk*

† Electronic Supplementary Information (ESI) available: [details of any supplementary information available should be included here]. See DOI: 10.1039/b000000x/

‡ Celebrating 300 years of Chemistry at Edinburgh.

1 (a) V. K Yachandra,, V. J. DeRose, M. J. Latimer, I. Mukerji, K. Sauer and M. P. Klein., *Science* 1993, **260**, 675. (b) V. J. DeRose, I. Mukerji, M. J. Latimer, V. K. Yachandra, K. Sauer and M. P. Klein,. *J. Am. Chem. Soc.* 1994, **116**, 5239. (c) G. Aromí, M. W. Wemple, S. J. Aubin, K. Folting, D. N. Hendrickson and G. Christou., *J. Am. Chem. Soc*., 1998, **120**, 5850. (d) T. Wydrzynski amd S. Satoh., *Photosystem II: The Light-Driven Water: Palstpoquinone Oxidoreductase;* Springer: Dordrecht, The Netherlands, 2005, p11. (e) J. Yano and V. K. Yachandra., *Inorg. Chem.*, 2008, **47**, 1711.

2 R. Sessoli, D. Gatteschi, A. Caneshi and M. A. Novak, *Nature,* 1993, **365**, 141. (b) R. Sessoli, H.-L. Tsai, A. R. Schake, S. Wang, J. B. Vincent, K. Folting, D. Gatteschi, G. Christou and D. N. Hendrickson. *J. Am. Chem. Soc.,* 1993, **115**, 1804.

3 (a) J.-P. Costes, J. M. Clemente-Juan, F. Dahan and J. Milon, *Inorg. Chem*. 2004, **43**, 8200-8202. (b) Y. G. Huang, X.-T. Wang, F. L. Jiang, S. Gao, M.-Y. Wu, Q. Gao, W. Wie and M. C. Hong., *Chem. Eur. J*. 2008, **14**, 10340. (c) E. Colacio, M. A. Palacios, A. Rodríguez-Díeguez, A. J. Mota, J. M. Herrera, D. Choquesillo-Lazarte and R. Clérac., *Inorg. Chem*., 2010, **49**, 1826. (d) M. Andruh, J.-P. Costes, C. Diaz and S. Gao., *Inorg. Chem*., 2009, **48**, 3342 and references herein.

4 (a) Y.-Z. Zheng, M. Evangelisti and R. E. P. Winpenny. *Angew. Chem. Int. Ed*., 2011, **50**, 3692. (b) M. Evangelisti, O. Roubeau, E. Palacios, A. Camón, T. N. Hooper, E. K. Brechin, J. A. Alonso. *Angew. Chem. Int. Ed.,* 2011, **50**, 1. (c) S. K. Langley, N. F. Chilton, B. Moubaraki, T. N. Hooper, E. K. Brechin and K. S. Murray. *Chem. Sci*., 2011, **2**, 1166. (d) G. Karotsis, M. Evangelisti, S. J. Dalgarno and E. K. Brechin. *Angew. Chem. Int. Ed.,* 2009, **48**, 9928.

5 (a) V. Mereacre, A. M. Ako, M. R. Clerac, W. Wernsdorfer, I. J. Hewitt, C. E. Anson, and A. K. Powell, *Chem. Eur. J.*, 2008, **14**, 3577. (b) T. C. Stamatatos, S. J. Teat, W. Wernsdorfer and G. Christou., *Angew. Chem. Int. Ed*., 2009, **48**, 521. (c) M. N. Akhtar, V. Mereacre, G. Novitchi, J.-P. Tuchagues, C. E. Anson, A. K. Powell, *Chem. Eur. J*., 2009, **15**, 7278. (d) J.-L. Liu, F.-S. Guo, Z.-S. Meng, Y.-Z. Zheng, J.-D. Leng, M.-L. Tong, L. Ungur, L. F. Chibotaru, K. J. Heroux and D. N. Hendrickson. *Chem. Sci.,* 2011, 2, 1268.

6 (a) J. Rinck, G. Novitchi, W. Van den Heuvel, L. Ungur, Y. Lan, W. Wernsdorfer, C. E. Anson, L. F. Chibotaru and A. K.

Powell. *Angew. Chem. Int. Ed.,* 2010, **49**, 7583. (b) A. Yamashita, A. Watanabe, S. Akine, T. Nabeshima, M. Nakano, T. Yamamura and T. Kajiwara. *Angew. Chem. Int. Ed.*, 2011, **50**, 1. (c) T. Peristeraki, M. Samios, M. Siczek, T. Lis and C. J. Milios. *Inorg. Chem.,* 2011, **50(11)**, 5175.

7 (a) T. N. Hooper, J. Schnack, S. Piligkos, M. Evangelisti and E. K. Brechin. *Angew. Chem. Int. Ed.,* 2012, **51**, 4633. (b) R. Inglis, E. Houton, J. Liu, A. Prescimone, J. Cano, S. Piligkos, S. Hill, L. F. Jones and E. K. Brechin. *Dalton Trans.,* 2011, 40, 9999.

8 (a) S. T. Meally, G. Karotsis, E. K. Brechin, G. S. Papaefstathiou, P. W. Dunne, P. McArdle and L. F. Jones., *CrystEngComm*., 2010, **12**, 59. (b) S. T. Meally, C. McDonald, G. Karotsis, G. S. Papaefstathiou, E. K. Brechin, P. W. Dunne, P. McArdle, N. P. Power and L. F. Jones. *Dalton Trans*., 2010, **39**, 4809. (c) S. T. Meally, C. McDonald, P. Kealy, S. M. Taylor, E. K. Brechin and L. F. Jones. *Dalton Trans.,* 2012, **41(18)**, 5610.

9 See also: Y.-L. Zhou, M.-H. Zeng, L.-Q. Wei, B.-W. Li and M. Kurmoo. *Chem. Mater*., 2010, **22**, 4295.

10 Examples include: (a) J. B. Vincent, C. Christmas, J. C. Huffman, G. Christou, H.-R. Chang and D. N. Hendrickson., *Chem. Commun.,* 1987, 236. (b) R. J. Kalawiec, R. H. Crabtree, G. W. Brudvig and G. K. Schulte., *Inorg. Chem.,* 1988, **27**, 1309. (c) J. B. Vincent, C. Christmas, H.-R. Chang, Q. Li, P. D. W. Boyd, J. C. Huffman, D. N. Hendrickson and G. Christou, *J. Am. Chem. Soc.,* 1989, **111**, 2086. (d) S. Wang, M. S. Wemple, J. Yoo, K. Folting, J. C. Huffman, K. S. Hagen, D. N. Hendrickson and G. Christou, *Inorg. Chem*., 2000, **39**, 1501. (e) G. S. Papaefstathiou, A. Escuer, C. P. Raptopoulou, A. Terzis, S. P. Perlepes, R. Vicente, *Eur. J. Inorg. Chem*., 2001, 1567. (f) D. J. Price, S. R. Batten, K. J. Berry, B. Moubaraki and K. S. Murray, *Polyhedron*, 2003, **22**, 165. (g) A. J. Tasiopoulos, W. Wernsdorfer, K. A. Abboud and G. Christou., *Inorg. Chem*., 2005, **44**, 6324. (h) H. Miyasaka, K. Nakata, L. Lecren, C. Coulon, Y. Nakazawa, T. Fujisaki, K. Sugiura, M. Yamashita and R. Clérac, *J. Am. Chem. Soc.,* 2006, **128**, 3770 (i) L. M. Wittick, L. F. Jones, P. Jensen, B. Moubaraki, L. Spiccia, K. J. Berry and K. S. Murray., *Dalton Trans*., 2006, 1534.

11 T. Cauchy, E. Ruiz and S. Alvarez., *J. Am. Chem. Soc*., 2006, **128**, 15722 and references herein.

12 (a) I. S. Tidmarsh, E. Scales, P. R. Brearley, J. Wolowska, L. Sorace, A. Caneschi, R. H. Laye, E. J. L. McInnes., *Inorg. Chem*., 2007, **46**, 9743. (b) R. P. Doyle, P. E. Kruger, B. Moubaraki, K. S. Murray and M. Nieuwenhuyzen, *Dalton Trans*., 2003, **22**, 4230. (c) E. Ruiz, J. Cano, S. Alvarez, and P. Alemany., *J. Am. Chem. Soc.*, 1998, **120**, 11122. (d) G. Chaboussant, R. Basler, H.-U. Güdel, S. Ochsenbein, A. Parkin, S. Parsons, G. Rajaraman, A. Sieber, A. A. Smith, G. A. Timco and R. E. P. Winpenny, *Dalton Trans.*, 2004, **17**, 2758.

13 Y. K. Gun'ko, U. Cristmann and V. G. Kessler., *Eur. J. Inorg. Chem.,* 2002, 1029.

14 V. L. Blair, W. Clegg, B. Conway, E. Hevia, A. Kennedy, J. Klett, R. E. Mulvey and L. Russo., *Chem. Eur. J*., 2008, **14**, 65.

15 C. Redshaw, D. Homden, D. L. Hughes, J. A. Wright and M. R. J. Elsegood. *Dalton Trans*., 2009, 1231.

16 C. E. Anson, W. Klopper, J.-S. Li, L. Ponikiewski and A. Rothenberger. *Chem. Eur. J*., 2006, **12**, 2032.

17 J.-P. Costes., L. Vendier and W. Wernsdorfer. *Dalton Trans.,* 2011, **40**, 1700.

18 S.-H. Zhang, N. Li, C.-M. Ge, C. Feng and L.-F. Ma, *Dalton Trans.,* 2011, **40**, 3000.

19 A. Escuer and G. Aromi, *Eur. J. Inorg. Chem.,* **2006**, 4721.

20 W. J. Evans,. R. E. Golden, and J. W. Ziller, *Inorg. Chem.*, 1993, **32**, 3041.

21 M. W. Wemple, D. M. Adams, K. Folting, D. N. Hendrickson and G. Christou. *J. Am. Chem. Soc*., 1995, **117**, 7275.

22 (a) E.-C. Yang, W. Wernsdorfer, L. N. Zakharov, Y. Karaki, A. Yamaguchi, R. M. Isidro, G.-D. Lu, S. A. Wilson, A. L. Rheingold, H. Ishimoto and D. N. Hendrickson. *Inorg. Chem*., 2006, **45**, 529. (b) J.-W. Ran, S.-Y. Zhang, B. Xu, Y. Xia, D. Guo, J.-Y. Zhang and Y. Ling., *Inorg. Chem. Commun.*, 2008, **11**, 73. (c) J. Lawrence, E.-C. Yang, R. Edwards, M. M. Olmstead, C. Ramsey, N. S. Dalal, P. K. Gantzel, S. Hill and D. N. Hendrickson. *Inorg. Chem.*, 2008, **47**, 1965. (d) D. Mandal, C. S. Hong, H. C. Kim, H.-K. Fun and D. Ray., *Polyhedron*, 2008, **27**, 2372. (e) Y. Xie, J. Ni, F. Zheng, Y. Cui, Q. Wang, S. W. Ng and W. Zhu. *Cryst. Growth and Design,* 2009, **9**, 118. (f) J. Zhang, P. Teo, R. Pattacini, A. Kermagoret, R. Welter, G. Rogez, T. S. A. Hor and P. Braunstein. *Angew. Chem. Int. Ed.,* 2010, **49**, 4443.

23 The ligand L_2H has been utilised elsehwere: (a) S.-H. Zhang, Y. Song, H. Liang and M.-H. Zeng. *CrystEngComm*., 2009, **11**, 865.

24 T. N. Hooper, J. Schnack, S. Piligkos, M. Evangelisti, E. K. Brechin, *Angew. Chem Int. Ed*., 2012, **51**, 4633.

25 W. H. Press, S. A. Teukolsky, W. T. Vetterling and B. P. Flannery, *Numerical Recipes in C: The Art of Scientific Computing*, Cambridge University Press, Cambridge, 2nd edn, 1992.

26 A. J. Blake, C. M. Grant, S. Parsons, G. A. Solan and R. E. P. Winpenny. *Dalton Trans.,* 1996, 321.

27 H. A. Z. Bethe, *Phys*. 1931, **71**, 205.

28 J. C Bonner, and M. E. Fisher, *Phys. Rev. A,* 1964, **135**, 640.

29 T. Birk, K. S. Pedersen, S. Piligkos, C. A. Thuesen, H. Weihe and J. Bendix. *Inorg. Chem.,* 2011, **50**, 5312.

30 R. D. Cannon and R. P. White, *Prog. Inorg. Chem.* 1988, **36**, 95 and references herein.

31 C. N. O'Callaghan and T. B. H. McMurry. *J. Chem. Res.,* 1988, **6** , 1549.